DOI of published article: https://doi.org/10.1016/j.clay.2020.105908

Molecular Mechanics of the Swelling Clay Tactoid Under Compression, Tension and Shear

H M Nasrullah Faisal[1], Kalpana S. Katti[1,2] Dinesh R. Katti[1,2,3]

[1]Department of Civil and Environmental Engineering, North Dakota State University, Fargo, ND 58108

[2]Center for Engineered Cancer Testbeds, North Dakota State University, Fargo, ND 58108

[3]Corresponding author, Dinesh.Katti@ndsu.edu, ph: 701-231-7245

Abstract

Montmorillonite is the principal constituent of many expansive soils. The swelling of expansive clays upon hydration can cause significant distress to infrastructure. On the other hand, the swelling characteristics lead to many beneficial applications of these clays, such as barrier materials and in nanocomposites. The montmorillonite hierarchical structure plays a vital role in the swelling of expansive clays. The hierarchical structure of montmorillonite consists of four levels, clay mineral layers, tactoids, aggregates, and assembly of aggregates. The clay tactoid is considered as the fundamental clay particle, which consists of several clay mineral layers stacked in the Z direction. We report here for the first time a molecular mechanics study of the clay tactoid. The molecular model of sodium-montmorillonite (Na-Mt) tactoid was built, and its mechanical properties were evaluated using Molecular Dynamics (MD) and Steered Molecular Dynamics (SMD) simulations. The mechanical response of Na-Mt tactoid was evaluated under compression, tension, and shear. Compression tests revealed a short linear characteristic with a compression modulus of 125 GPa followed by a nonlinear portion with increasing modulus approaching 640 GPa, which is the modulus of a single clay mineral layer. The tensile pulling of the tactoid also indicated an influence of the tactoid nanostructure with the influence of multiple neighboring layers of tactoid. The shearing simulations indicated first a mechanical response with a modulus of 10 GPa ending with locking of interlayer cations into tetrahedral cavities followed by small displacements exhibiting a modulus of 70 GPa. All of the mechanical behaviors were related to the evaluated interaction energies between clays and cations during loading. These studies elucidated key mechanisms of swelling clay tactoid response to loading.

Keywords: clay, molecular dynamics, tactoid, binding energy, tension, compression, shear.

1. Introduction

Evaluation and prediction of reactive soil response is a topic of great interest among the researchers. These soils undergo significant changes in volume and microstructure under certain environmental conditions. There are three major types of reactive soils; expansive, collapsible, and chemically reactive. Expansive soils are found extensively in the USA and also in other parts of the world. In the case of expansive soils, the dramatic volume change, degradation of shear strength upon swelling, and the development of considerable swelling pressures when constrained, cause enormous damage to the infrastructure, including distress to buildings, foundations, highways, dams, etc. Smectite clays such as montmorillonite constitute a significant portion of expansive soils. Montmorillonite swells significantly upon interaction with water. Under free swell conditions, montmorillonite can expand as much as 15 times its original volume. However, if the swelling is constrained, it exerts a large amount of swelling pressure (Buzzi et al., 2010; Grim, 1968; Katti et al., 2002). As a swelling clay, montmorillonite also has beneficial applications in geoenvironmental engineering, polymer clay nanocomposites, pharmaceutical, cosmetics, and the petroleum industry.

Montmorillonite is a member of the smectite group. Clay minerals are defined as fine-grained, earthy, and natural materials that exhibit plasticity with the addition of water (Guggenheim and Martin, 1996). Smectite clay belongs to the aluminum phyllosilicate group, with a varying combination of tetrahedral silica sheet (t) and octahedral alumina sheet (o). Sodium montmorillonite (Na-Mt) is a 2:1 (t-o-t) phyllosilicate mineral with an alumina octahedral sheet sandwiched between two tetrahedral silica sheets (Grim, 1942; Hendricks and Jefferson, 1938). Isomorphous substitution of aluminum ions from the octahedral sheet causes the development of

negative charge, which is balanced by different interlayer cations (for example, Na, Mg, K, Ca, Cs).

The swelling of Na-montmorillonite is characterized by structural changes both at the nano and micro scale. Clay interlayer space increased with an increasing amount of hydration in the nanometer dimension (Pradhan et al., 2015). The breakdown of Na-Mt particle occurred during swelling (Katti and Shanmugasundaram, 2001). Discrete element modeling (DEM) study on swelling clays simulated particle breakdown (Katti et al., 2009). To bridge the swelling behavior between the nano and micro scale, modeling of the clay structure at intermediate levels is essential. According to earlier studies, Na-montmorillonite possesses a hierarchical structure. Investigation of clay porosities using scanning electron microscopy (SEM), small-angle X-ray scattering (**SAXS**), X-ray powder diffraction (**XRD**), and mercury intrusion porosimetry (**MIP**) highlighted three sizes of porosities, interlayer porosity, inter-particle porosity and inter-aggregate porosity (Bihannic et al., 2001; Cases et al., 1992; Keller et al., 2013; Likos and Wayllace, 2010; Massat et al., 2016). Analysis of the difference between hydration of clay-rich soils and hydration of porous granular soils led to the understanding of the multiscale structure of clays (Jullien et al., 2005; Norrish, 1954; Pusch and Yong, 2003; Sposito and Prost, 1982; Yong, 1999). This multiscale structure consists of the microscopic scale (t-o-t layer), mesoscopic scale (stacks of t-o-t layers), and macroscopic scale (a random combination of stacks). The hierarchical structure of smectite (layer, particle, single aggregate, multiple aggregates) was also described for defining its various hydration sites as a function of scale (Perdrial and Warr, 2011). Thermoporometric study of mesoscopic swelling of Na-Mt clay mineral, also referred to its stratified architecture (Salles et al., 2008; Salles et al., 2009). Based on these observations, we can state that the hierarchical structure of Na-Mt clay mineral is composed of four levels.

- Unit clay mineral layer: T-O-T sheet structure with interlayer sodium cations.
- Tactoid: Several clay mineral layers (about 10) stacked one over other in the Z direction to form a clay tactoid.
- Aggregate: Several clay tactoids are gathered in different orientations to form a clay aggregate.
- Multiple aggregate/ Assembly of aggregates: Some clay aggregates are combined to form a multiple-aggregate.

The unit clay mineral layers (t-o-t) of Na-Mt clay mineral form a stack along the vertical (Z) direction. This stack is termed as clay tactoid. Clay tactoid structure is often viewed as the characteristic feature of consolidated natural bentonite bed where significant overloading yields the alignment of clay mineral layers into stacks. Previous X-ray diffraction studies showed the formation of Na-Mt clay tactoids containing ten clay mineral layers stacked to each other in the Z-axis (Jonas and Oliver, 1967). However, the number of clay mineral layers in a tactoid varies in aqueous solutions with varying ion concentration. Increased ionic concentration (salinity) results in tactoids having higher number of clay mineral layers. Na-montmorillonite tactoid was seen to have 5 to 20 clay mineral layers in solution depending upon the NaCl concentration with an average of 10 clay mineral layers (Pusch et al., 1990). Clay tactoid structure is also affected by the relative humidity (RH). Nitrogen adsorption study of montmorillonite showed that the hydration at RH of 100% caused the increment of both total clay mineral surface area and micropore (interlayer) surface area i.e. decreased number of clay mineral layers in tactoid (Neaman et al., 2003). Clay tactoid also behaves as the primary clay particle, which forms aggregates upon organization in different orientations. In the present study, tactoid will be considered to be made up of ten clay mineral layers.

Researchers evaluated different properties of clay minerals through experimental and computational approaches. Influence of temperature, pressure, humidity etc. on clay minerals were investigated to better understand the impact of these environmental factors on the mechanical properties of clays (Lloret et al., 2003; Pellet et al., 2013; Rajini et al., 2013; Villar and Lloret, 2004; Wang et al., 1979). Molecular dynamics (MD) simulations have long been utilized by the researchers to investigate various geological materials as well as clay minerals, to predict the time-dependent behavior of molecular systems (Chang et al., 1995; Faisal et al., 2020; Karaborni et al., 1996; Katti et al.; Katti et al., 2015; Shroll and Smith, 1999; Skipper et al., 1995b; Smith et al., 2004; Teppen et al., 1997; Thapa et al., 2020). MD simulations were also used to model the hydration behavior of swelling clay minerals (Rahromostaqim and Sahimi, 2018; Sun et al., 2015; Tao et al., 2010; Thapa et al., 2020). Nanoscale bending of clay mineral layers and their relationship with cation exchange capacity (CEC) and terminal shear stress were investigated by different researchers (Fu et al., 2011; Zartman et al., 2010). Steered molecular dynamics (SMD) technique was utilized to evaluate the mechanical response of Na-Mt clay mineral (Katti et al., 2005a; Katti et al., 2005b, 2007; Schmidt et al., 2005). The approach behind performing steered molecular dynamics (SMD) is that initially, a subset of atoms is fixed. In contrast, another subset of atoms is pulled/pushed with predetermined constant-velocity or constant-force, and the response of the molecule is recorded. Interactions of various fluid molecules with clay minerals were also studied using molecular dynamics (MD) to evaluate the effect of fluid polarity on swelling (Katti et al., 2017a; Katti et al., 2018). The swelling of Na-Mt clay mineral interlayer spaces inside Na-Mt clay tactoids contributed to the swelling of the tactoid and the clay (Perdrial and Warr, 2011). Clays are subject to a variety of loading paths such as compression, tension, and shear during construction and operation of civil infrastructure components such as structures, excavations,

tunnels, etc. Since clay tactoids are fundamental building blocks of clay aggregates, modeling Na-Mt clay tactoid subject to various loading paths will provide quantitative parameters and an insight into the response of the clay tactoid under various loading conditions. The present study seeks to evaluate the mechanical properties of Na-Mt clay tactoid and investigate molecular-scale mechanisms during loading using both MD and SMD.

2. Methodology

2.1. Modeling approach

The authors have performed various experimental and modeling studies on Na-montmorillonite (SWy-2) obtained from clay mineral repository at the University of Missouri, Columbia (Katti and Shanmugasundaram, 2001; Katti et al., 2007; Schmidt et al., 2005). Although the structural formula of this Na-montmorillonite is,

$$(Ca_{0.12}Na_{0.32}K_{0.05})[Al_{3.01}(III)_{0.41}Mn_{0.01}Mg_{0.54}Ti_{0.02}][Si_{7.98}Al_{0.02}]O_{20}(OH)_4$$

(Van Olphen and Fripiat, 1979), a simplified version $NaSi_{16}(Al_6FeMg)O_{20}(OH)_4$ was utilized for model construction. Previously proposed coordinates (Skipper et al., 1995a), partial charges (Teppen et al., 1997), and CHARMm force field parameters (Katti et al., 2005b; Schmidt et al., 2005) were used. Isomorphous substitution occurred in the octahedral sheet (o) as one out of every four Al^{3+} ions was replaced by Mg^{2+} or Fe^{3+} ions. The development of negative charge in the clay mineral layer due to isomorphic substitution was neutralized by introducing interlayer Na cation.

The present study utilized the Na-Mt 6×3 clay model as used in several previous studies (Katti et al., 2017a; Katti et al., 2017b; Katti et al., 2018). The unit cell dimensions of the clay mineral layer were 5.28 Å×9.14 Å×6.56 Å. Hence, the initial overall dimensions of single 6×3 Na-Mt clay

mineral layer (t-o-t) were 31.68 Å×27.44 Å×6.56 Å (**Fig. 1**). The initial interlayer space was 3.44 Å, which resulted in the initial d-value of 10 Å. Each 6×3 clay mineral layer contained 720 atoms. As isomorphic substitution generated a charge of -0.5 e in each unit cell, nine interlayer Na cations were introduced in the interlayer space to balance the charge of the 6×3 clay model.

Figure 1

For building the model of Na-Mt clay tactoid, ten 6×3 clay mineral layers were stacked on top of each other in the Z direction. These ten layers were identified as B, C, D, E, F, G, H, I, J, and K layer from bottom to top along the Z-axis, respectively (**Fig. 2**). This model contained nine interlayer spaces. The initial vertical (Z) dimension of Na-Mt clay tactoid was 96.56 Å, the summation of the thickness of 10 clay mineral layers (10×6.56 Å) and nine interlayer spaces (9×3.44 Å). The overall dimensions of Na-Mt clay tactoid were 31.68 Å×27.44 Å × 96.56 Å. Each interlayer space contained nine Na cations. Thus, the full Na-Mt clay tactoid model had 7281 atoms (7200 clay atoms and 81 interlayer Na cations). The distance between the top and bottom clay mineral layers was termed as the 'aggregated d-value' as it was the sum of all the d-values within the Na-Mt tactoid. The initial magnitude of the 'aggregated d-value' was 90 Å. Materials Studio 7.0 was used to build the Na-Mt clay tactoid model.

Figure 2

Na-Mt clay tactoid was parameterized using CHARMm (Chemistry at HARvard Macromolecular Mechanics) force field (Vanommeslaeghe et al., 2010). A set of functions and associated constants were utilized to describe the energy expression of a molecular system using the CHARMm force field. Consistent force field (CFF) parameters of Na-Mt, developed in an earlier study by MP2 ab intio calculations (Teppen et al., 1997) were transformed to the CHARMm force field (Schmidt et al., 2005) and used in this study. A handful of empirical force fields were utilized by researchers to model various properties of different clay minerals. ClayFF, CementFF, ReaxFF, URF, InterfaceFF etc. are the most commonly used force fields for modeling clay behavior. To facilitate the comparison of these force fields in a single platform, a couple of online force field databases were introduced in a user-friendly manner (Emami et al., 2014; Mishra et al., 2017). However, comparing the performance of force fields is not a straightforward task as it was influenced not only by the accurate reproduction of experimental observables by fitted parameters but also by their computational efficiencies. ClayFF and InterfaceFF were considered the simplest (easily implementable) and most reliable (in terms of partial charges) force fields respectively while ReaxFF was treated as the most unique due to its ability of modeling bond breaking/formation. This particular behavior of ReaxFF limited its capability of modeling the mechanical response (Mishra et al., 2017). The present study investigated the mechanical response of tactoid which in turn depends on its non-bonded interactions. Therefore, InterfaceFF would be the most suitable option for modeling clay non-bonded interactions. The InterfaceFF force field parameterization was validated by PCFF potential energy expression which employed semiempirical charge equilibration (instead of ab-initio calculations like CFF) to obtain the partial atomic charges of montmorillonite (Heinz et al., 2005). This semiempirical method was based

upon the extended Born model that accounted for both the covalent and ionic bonding through the exploitation of atomization and ionization energies respectively (Heinz and Suter, 2004). The partial charges used by the present clay tactoid modeling study (unaltered CFF charges) fell within the range of maximum possible deviations of PCFF semiempirical procedure ($\pm$0.3 e). Therefore, this model efficiently depicted the correct non-bonded interactions within the tactoid like InterfaceFF. The current clay CHARMm parameters were extensively validated with experimental results and other modeling results in the literature and by previous studies (Katti et al., 2005a; Katti et al., 2005b; Katti et al., 2006; Pradhan et al., 2015).

2.2. Simulation details

The MD and SMD simulations of Na-Mt clay tactoid were performed using NAMD 2.12 (Phillips et al., 2005). NAMD was developed by the Theoretical and Computational Biophysics Group in the Beckman Institute for Advanced Science and Technology at the University of Illinois at Urbana-Champaign. All the simulations were run on the Center for Computationally Assisted Science and Technology (CCAST), a parallel computing facility at North Dakota State University. The simulations utilized one node and twenty Intel Xeon 2.5 GHz processors with 15GB DDR3 RAM at 1866 MHz.

The Na-Mt tactoid model was first minimized under vacuum conditions (0 K temperature and 0 kPa pressure) using a conjugate gradient method (Payne et al., 1992). Next, the model was brought to normal temperature (300 K) and pressure (101.325 kPa) conditions using a stepwise approach. The normal temperature (300 K) was raised from 0 K in three steps (100 K/step). Next,

the normal pressure condition (101.325 kPa) was achieved from 0 kPa in four steps (25 kPa/step). The Na-Mt tactoid model simulation was conducted at NTP condition (isobaric-isothermal) for 2 ns to attain the equilibrium condition. As the time step used for MD simulation is 0.5 fs, the model was run at NTP for 4,000,000 steps. All of the MD simulations of Na-Mt tactoid were performed using the periodic boundary conditions (PBC) to implement the Particle Mesh Ewald (PME) electrostatic interactions.

The equilibrated Na-Mt tactoid model was then utilized to evaluate its mechanical response. The tactoid model was subjected to three loading paths, compression, tension, and shear to evaluate the mechanical properties under these loading conditions. The compressive behavior of tactoid was investigated by applying increasing magnitudes of compressive forces on the top clay mineral layer oxygen atoms (layer K) and by keeping the bottom clay mineral layer (layer B) fixed. The forces applied on each oxygen atom of top clay mineral layer (K) were 0-100 pN in increments of 25 pN followed by increments of 50 pN to 300 pN and up to 2500 pN in increments of 100 pN. The stresses equivalent to these forces were calculated to be ranging from 0 to 37 GPa in 31 increments. Constant force SMD was used to apply these forces on Na-Mt clay tactoid. The d-values of tactoid were measured after these constant-force SMD simulations reached equilibrium conditions for a given load. The d-values were computed by tracking the coordinates of the bottom oxygen atoms of each clay mineral layer. Constant-velocity compression on Na-Mt tactoid was also performed using steered molecular dynamics (SMD) to determine the characteristic spring constant (k) and pulling velocity (v) of the tactoid. These values were determined by utilizing the constant-force compression response. A number of constant-velocity SMD (compression) simulations were performed on clay tactoid utilizing the combinations of various magnitudes of spring constants (k= *3, 5, 7, and 9 kcal/mol/Å*^{2}) and velocities (v=*0.5, 1, 1.5, 2, and 2.5 Å/ps*).

The specific combination of spring constant (k) and velocity (v) that provided the identical compression behavior to the constant-force compression was taken as the characteristic spring constant and velocity of tactoid. The values were found to be $k=9$ *kcal/mol/Å*^{2} and $v=2$ *Å/ps*, respectively, and further utilized to investigate the tensile and shear properties of tactoid.

In order to investigate the tensile properties of Na-Mt tactoid (stress required to pull off the various number of clay mineral layers from tactoid), tensile (pulling) forces were applied on the top 1 (K), 2 (J, K) and 3 (I, J, K) clay mineral layers by keeping the bottom layer (B) fixed. Constant-velocity SMD ($k=9$ *kcal/mol/Å*^{2}, $v=2$ *Å/ps*) was utilized to apply tensile forces. The shearing behavior of Na-Mt tactoid was also studied using constant-velocity SMD ($k=9$ *kcal/mol/Å*^{2}, $v=2$ *Å/ps*). We applied force on the surface of the top clay mineral layer (K) along the X-axis while keeping the bottom clay mineral layer (B) fixed, followed by measuring the corresponding shear deformation.

3. Results

3.1. Equilibrated Na-Mt tactoid

The equilibrated Na-Mt tactoid model after 2 ns of simulation at NTP condition (300 K and 101.325 kPa) is shown in **Fig. 3**.

Figure 3

The final height of equilibrated Na-Mt tactoid was 104.04 Å, as opposed to the initial height of 96.56 Å. The final dimensions of Na-Mt tactoid were 33.66 Å×29.08 Å×104.04 Å. The increase

in tactoid height resulted from the increase in the interlayer space. The initial and equilibrated aggregated d-value was 90 Å and 97.2 Å, respectively (**Fig. 3**). The change in the thickness of the clay mineral layer was thus minimal (from 6.56 Å to 6.65 Å).

Table 1

Table 1 shows the d-values between each pair of clay mineral layers at equilibrium. As seen, the d-values were quite similar throughout the tactoid, and the layers were parallel to one another. The mean d-value of tactoid was 10.795 Å (≈ 10.80 Å). This was consistent with the previously reported magnitude of d-values from experimental and modeling studies (Amarasinghe et al., 2008; Katti et al., 2005a; Pradhan et al., 2015). The average interlayer space was observed to be 4.15 Å. Application of XRD techniques on montmorillonite performed by other researchers provided basal spacing values ranging from 9.6 Å to 12.4 Å (Ferrage et al., 2005; Lin, et al., 2001; Liu, et al., 2011).

Further, the non-bonded interaction energies for clay mineral layers inside the Na-Mt tactoid were calculated. Non-bonded interaction energies consist of electrostatic and Van der Waals (VDW) interaction energies. Positive and negative values of the energies referred to repulsive and attractive interaction energies, respectively. Non-bonded energies between each pair of clay mineral layers are shown in **Table 2**.

Table 2

As seen, the clay mineral layers in the tactoid had relatively uniform attractive pairwise interactions between them with an average value of -1850 kJ/mol. The electrostatic interactions between the clay mineral layers were repulsive, while the Van der Waals interactions were attractive. The average value of Van der Waals energy (-2599 kJ/mol) was found to be 3.5 times greater than average electrostatic energy (749 kJ/mol). Non-bonded energy was also computed for each clay mineral layer to identify its interactions with interlayer Na cations in Na-Mt tactoid.

Table 3

Table 3 indicates that all the clay mineral layers except the top (K) and bottom (B) layers had a similar magnitude of interaction energy with interlayer cations. The interaction energies of interlayer Na cations with top and bottom clay mineral layers were almost one-half (3642 kJ/mol) compared to the interactions with the remaining clay mineral layers (6556 kJ/mol). This difference in the interaction energy occurred because the top and bottom clay mineral layers contained Na cations just on one side of the clay mineral layer, while the other clay mineral layers had cations on both sides. The attractive electrostatic energies were much higher than the repulsive Van der Waals energies among the Na ion and clay mineral layer interaction energies.

The binding energy of a single clay mineral layer to its tactoid is described as the total of Van der Waals and electrostatic energies acting between the clay mineral layer and the rest of the tactoid (other clay mineral layers and interlayer cations). Binding energy reflects how strongly a clay mineral layer is bonded to other constituents in the tactoid.

Table 4

The calculated binding energies of the top (K) and bottom (B) clay mineral layers were about 53% of the binding energies of remaining individual clay mineral layers **(Table 4)**. This difference was attributed to the position of the clay mineral layer in the tactoid (top/bottom), the number of interlayer cations interacting with the clay mineral layer, and adjacent clay mineral layer interactions. Electrostatic and Van der Waals energies contributed to about the same order of magnitude to the binding energies of clay mineral layers and both imparted attractive interactions. The total attractive interaction energy between interlayer cations and all the clay mineral layers was -59738 kJ/mol. These results also highlighted the role of other clay mineral layers and Na ions in other interlayers on the binding energy of a clay mineral layer within the tactoid. The binding energy of a single clay mineral layer was higher than its pairwise interactions with adjacent clay mineral layers and cations due to the influence of other clay mineral layers and Na ions in the tactoid.

3.2. Compressive Loading on Tactoid

The response of Na-Mt tactoid under an increasing amount of compression was evaluated in the present study. Significant changes occurred in the interlayer space of tactoid due to the application of the compressive stresses. Changes in clay mineral layer thicknesses were minimal. The relationship between increasing compressive stress and aggregated d-value and the resultant stress-strain curves were shown in **Fig 4.**

With the increasing amount of stress, the aggregated d-value of Na-Mt tactoid decreased (**Fig. 4a**). This reduction was the result of the decrease in the interlayer spaces between each pair of clay

mineral layers inside the tactoid. The reduction in interlayer space solely contributed to the lessening of d-values between clay mineral layers, since the decrease in clay mineral layer thickness was insignificant. The equilibrated aggregated d-value of Na-Mt tactoid under the compression of 0 GPa was 97.2 Å. As the applied stress increased from 0 GPa to 29.6 GPa, the aggregated d-value gradually decreased from 97.2 Å to 89.10 Å. The Na-Mt tactoid model was deformed at the most by about 8.1 Å under compression because, at this magnitude of compressive stress (29.6 GPa), the interlayer distance approached the Van der Waals radius distance between the clay mineral layers. The stress-strain behavior of Na-Mt tactoid due to compression loading was also determined (**Fig. 4b**).

Figure 4

The amount of deformation in aggregated d-value was divided by the initial height of equilibrated tactoid to compute the strain values. This stress-strain plot was primarily composed of two different regions i.e. lower modulus (linear) region and higher modulus (non-linear) region. Within the initial linear region from 0 to 2.22 GPa, the Na-Mt tactoid exhibited a compression modulus of 125 GPa (**Fig. 4b**). The apparent non-linear higher modulus region (2.22-29.6 GPa) actually consists of three different linear zones. The compression moduli of Na-Mt tactoid was caclculated as 237.5 GPa, 411 GPa and 643 GPa for the stress regions of 2.22-5.92 GPa, 5.92-14.8 GPa and 14.8-29.6 GPa respectively, as shown in **Table 5**. One of the previous studies from the author's group reported the elastic modulus of clay mineral layer as 696.55 GPa through constant-force SMD simulations (Sikdar et al., 2008). Previously proposed bulk amorphization strength of montmorillonite (60 GPa) validated the compression strength of tactoid as of 29.6 GPa (Zartman et al., 2010). Moreover, modulus mapping experiment of clay determined the elastic modulus as

346 of 352.9 GPa, which was the same order of magnitude of derived modulus of tactoid (643 GPa)
347 (Sikdar et al., 2008).

348

349 **Table 5**

350

351 A snapshot of the Na-Mt tactoid model at 29.6 GPa of stress, having an aggregated d-value of
352 89.10 Å, is shown in **Fig. 5**.

353 **Figure 5**

354

355 **Table 6** shows the d-values between each pair of clay mineral layers inside Na-Mt tactoid
356 under 29.6 GPa of compression.

357 **Table 6**

358

359 The top clay mineral layer (H, I, J, and K) interlayers were deformed more, shown by lower
360 d-values while bottom clay mineral layers (B, C, D, and E) were deformed relatively less,
361 demonstrated by higher d-values. Hence the top portion of tactoid was more deformed than the
362 bottom portion of tactoid under compression. The extent of interlayer deformation decreased
363 successively from top to bottom along the tactoid. The minimum interlayer deformation (0.77 Å)
364 occurred between the bottom clay mineral layers (B and C), while the maximum interlayer
365 deformation (0.95 Å) took place between the top clay mineral layers (J and K).

3.3. Tensile Loading on Tactoid

The top clay mineral layers of equilibrated Na-Mt tactoid were pulled in the vertical direction to observe the tensile deformation of tactoid. The relationship between the pulling stress and displacement of top clay mineral layers is shown in **Fig 6.** In the case of pulling of only the topmost clay (K) layer, the layer was linearly displaced with increasing stress up to peak stress of 2.87 GPa, which occurred at a displacement of 8.15 Å. As the clay mineral layer moved beyond this distance, the pulling stress required to displace the top clay mineral layer started to reduce, indicating the detachment initiation of the top clay mineral layer from the rest of the tactoid. The interactions between the top clay mineral layer and the rest of the tactoid diminished linearly with the further displacement of the top layer (K).

Figure 6

With the pulling of top two (J, K) and three (I, J, K) clay mineral layers, the peak stress occurred at a distance of about 8.1 Å, a magnitude similar to the case of pulling only the top clay mineral layer (**Fig. 6b**). However, with the increased number of clay mineral layers being pulled, the magnitude of the maximum pulling stress increased (3.15 GPa for top two clay mineral layers and 3.45 GPa for top three clay mineral layers). The modulus values for tensile pulling of clay mineral layers from the tactoid were 133 GPa for one clay mineral layer (K), 170 GPa for pulling two clay mineral layers (J, K), and 187 GPa for pulling top three clay mineral layers (I, J, K). Beyond a displacement of 20 Å, we observed rigid body motion of the pulled clay mineral layers.

3.4. Shear Loading on Tactoid

The shearing of Na-Mt tactoid was performed by pulling the topmost clay mineral layer (K) along its horizontal direction while the bottom layer (B) was fixed (**Fig. 7**). Upon the application of a constant horizontal pulling velocity of 2 Å/ps, we observed a compound response from the clay tactoid.

Figure 7

During the application of shear stress on Na-Mt tactoid, the clay mineral layers slided relative to each other except the fixed bottom layer (layer B). This gradual sliding of clay mineral layers deformed the top portion of tactoid the most and bottom portion least, i.e., the distance traveled by the top and bottom clay mineral layers were the largest and smallest, respectively. At the end of the shearing, the top clay mineral layer (K) was horizontally displaced by a total of 47.95 Å to its initial position (**Fig. 7**). The shear stress-displacement plot of top clay mineral layer K is presented in **Fig. 8**.

Figure 8

This plot displays two distinct phases of tactoid response (sliding of clay mineral layers) due to applied shear stress. The displacement of top clay mineral layer K from 0 Å to 44.8 Å reflected the first phase of the response. During this phase, the stress increased from 0 GPa to 4.2 GPa. The average horizontal relative displacement between each of the clay mineral layers at the end of this phase was about 4.98 Å. After the "first shearing" phase, as the shearing continued, very small (0.30 Å), relative displacements (second phase) between the clay mineral layers were observed. In the shear stress-displacement plot (**Fig. 8**), the second phase was reflected by the steep response of curve where the shear stress sharply increased from 4.2 GPa to 6.87 GPa over the displacement

409 of 3.15 Å of the top clay mineral layer K. Upon further application of constant horizontal velocity
410 to the top clay mineral layer K, the magnitude of shear stress dropped almost linearly
411 characterizing the complete separation of the top clay mineral layer from the tactoid. During the
412 entire shearing of tactoid, the second from bottom clay mineral layer (C) moved by 5.26 Å in the
413 horizontal direction while the topmost layer (K) moved by 47.95 Å. The total displacement of the
414 top clay mineral layer (layer K) was transformed into the shear strain of tactoid considering the
415 equilibrium height (104.04 Å) of the clay tactoid. Based on the observed response, two different
416 shear moduli for the tactoid, representing the two phases of observed shear deformations, were
417 computed as 10 GPa and 69.56 GPa, respectively. The first phase of shearing (0-4.2 GPa) was the
418 initial elastic shearing of tactoid as the withdrawal of stress brought back the initial tactoid
419 conformation. The second phase of shearing (4.2-6.87 GPa) indicated the transition from elastic
420 to plastic deformation, where the interlayer cations that moved into the tetragonal cavities resisted
421 the deformation through strong binding interactions with clay mineral layers inside the tactoid.
422 During the first phase of shearing, the clay mineral layers smoothly slided past each other as the
423 interlayer cations moved along the direction of shear. This translation of cations allowed the
424 gradual sliding of clay mineral layers from top (K) to bottom (C). The cations in the bottom
425 interlayer space (between B and C layers) got locked up in the tetrahedral cavities after certain
426 amount of translation which in turn initiated the locking of the sliding phenomena of clay mineral
427 layers. Eventually, the clay mineral layers gradually got locked up from bottom (C) to top layer
428 (K) along the tactoid. This specific locking incidence specified the steep shearing response of
429 tactoid. However, the continuous pulling of top clay mineral layer K eventually overcame its
430 binding with the rest of the tactoid and thereby caused its separation.

431

4.0 Discussion

Inside a Na-Mt tactoid, attractive short-range (Van der Waals) interactions were predominant between clay mineral layers. The attractive interactions between interlayer sodium cations and clay mineral layers are dictated by long-range (electrostatic) interactions. The clay mineral layers located at the two extremes of tactoid (top and bottom) were more loosely bonded as observed by their lesser interactions with interlayer cations. These interactions can be compared with experimental data by computing energy per surface area for both the pairwise interactions between the clay mineral layers (**Table 2**) and their total binding interactions with rest of the tactoid (**Table 4**). The computed values of energy per surface area, 311 mJ/m^2 for pairwise interactions and 928 mJ/m^2 for total binding interactions for a clay mineral layer within the tactoid are found. These values are of the same order of magnitude as the previously reported values i.e. 424 and 205 mJ/m^2 (Douillard et al., 2007; Helmy et al., 2003). The maximum compression of Na-Mt tactoid was observed to be dependent upon the Van der Waals radii of tetrahedral oxygen atoms of clay mineral layers. During the compression of tactoid, interlayer Na cations occupied the ditrigonal cavities of clay mineral layers. The Van der Waals radii of tetrahedral oxygen atoms were found to be 1.6 Å. Thus, the effective interlayer space was computed as 0.95 Å by subtracting the VDW radius (1.6 Å) of tetrahedral oxygen atoms from both sides of the interlayer space (4.15 Å) (**Fig. 9**). The compression of Na-Mt tactoid was the result of the reduction in interlayer space. The maximum possible decrease in interlayer space was equal to the magnitude of effective interlayer space (0.95 Å) (**Table 5)**.

Figure 9

In the current study, multiple values of compression moduli were found during the clay tactoid compression. The lower modulus region (0-2.22 GPa) characterized the initial compression of the interlayer space. On the other hand, the higher modulus region (>2.22-29.6 GPa) reflected the full compression of effective interlayer space and the beginning of the compression of the clay mineral layers. The aggregated d-value of Na-Mt tactoid was reduced by 8.1 Å under maximum compression (29.6 GPa). The tensile pulling of a different number of top clay mineral layers caused the permanent separation of them from tactoid beyond 8.15 Å displacement and almost nullified Na-clay mineral layer attractive interactions. In the case of tensile pulling of Na-Mt tactoid, the magnitude of required pulling stress to completely detach the clay mineral layer gradually increased with the number of pulled clay mineral layers. Pulling off one clay mineral layer (K) required 2.87 GPa while pulling off three clay mineral layers (I, J, K) required 3.45 GPa as three clay mineral layers had higher non-bonded interactions with the rest of the tactoid compared to just one clay mineral layer with rest of tactoid. Horizontal shearing of the tactoid consisted of two distinct phases. In the first phase, each clay mineral layer slided to the same extent 4.98 Å and got locked. The locking was consecutive from the top layer to the bottom layer. The locking occurred when the sodium ions migrated to tetragonal cavities of the clay mineral layers. When the bottom layer was locked, it represented the end of phase I. With the continued increase in shear stress, a very small shear deformation of 0.3 Å was observed. This phase was represented by a much steeper slope than Phase I. The two phases exhibited moduli of 10 GPa and 69.56 GPa, respectively. Further, phase II ended when the top clay mineral layer was separated from the tactoid resulting in the negative slope of the plot, as shown in Figure 8.

5.0 Conclusions

In the present study, for the first time, a molecular model of Na-Mt tactoid is developed and subjected to mechanical loading. We have used molecular dynamics (MD) simulations to evaluate the interaction energies within the equilibrated tactoid and steered molecular dynamics (SMD) simulations to investigate the mechanical response of Na-Mt tactoid under compression, tension, and shear loadings. The key findings are summarized below:

1. In equilibrated Na-Mt tactoid, pairwise non-bonded interactions between the clay mineral layers are identical and attractive in nature. The attractive Van der Waals interactions dominate the total energy as compared to the repulsive electrostatic interactions between the clay mineral layers. The non-bonded interaction energies between the interlayer cations and clay mineral layers at the top and bottom of the tactoid are almost one-half of the interaction energies between cations and other clay mineral layers.
2. During compression, the maximum deformation of the interlayer space is significantly less than the d-value of the interlayer and is dictated by the effective interlayer space.
3. Pulling off an increasing number of clay mineral layers from tactoid requires larger stress.
4. The application of the shear stress to the top of the tactoid results in a relatively uniform displacement of clay mineral layers, with respect to the adjacent layers.
5. Compressive, tensile, and shear moduli of the clay tactoid are computed, and the values depend upon the magnitude of applied stress.

Acknowledgments

The authors would like to acknowledge the financial support from the US Department of Transportation Mountain-Plains Consortium (MPC) Grant #: DTRT13-G-UTC38. We also recognize the computational facilities provided by North Dakota State University Computationally Assisted Science and Technology (CCAST), and the support of NSF MRI grant #1229316 and NSF OIA NDACES-1946202

Conflict of Interest

On behalf of all authors, the corresponding author states that there is no conflict of interest.

References

Amarasinghe, P.M., Katti, K.S., Katti, D.R., 2008. Molecular Hydraulic Properties of Montmorillonite: A Polarized Fourier Transform Infrared Spectroscopic Study. Applied Spectroscopy 62, 1303-1313.

Bihannic, I., Tchoubar, D., Lyonnard, S., Besson, G., Thomas, F., 2001. X-ray scattering investigation of swelling clay fabric 1. The dry state. Journal of Colloid and Interface Science 240, 211-218.

Buzzi, O., Fityus, S., Sloan, S.W., 2010. Use of expanding polyurethane resin to remediate expansive soil foundations. Can. Geotech. J. 47, 623-634.

Cases, J.M., Berend, I., Besson, G., Francois, M., Uriot, J.P., Thomas, F., Poirier, J.E., 1992. MECHANISM OF ADSORPTION AND DESORPTION OF WATER-VAPOR BY HOMOIONIC MONTMORILLONITE .1. THE SODIUM-EXCHANGED FORM. Langmuir 8, 2730-2739.

Chang, F.R.C., Skipper, N.T., Sposito, G., 1995. COMPUTER-SIMULATION OF INTERLAYER MOLECULAR-STRUCTURE IN SODIUM MONTMORILLONITE HYDRATES. Langmuir 11, 2734-2741.

Douillard, J.M., Salles, F., Devautour-Vinot, S., Manteghetti, A., Henry, M., 2007. Study of the surface energy of montmorillonite using PACHA formalism. Journal of Colloid and Interface Science 306, 175-182.

Emami, F.S., Puddu, V., Berry, R.J., Varshney, V., Patwardhan, S.V., Perry, C.C., Heinz, H., 2014. Force Field and a Surface Model Database for Silica to Simulate Interfacial Properties in Atomic Resolution. Chemistry of Materials 26, 2647-2658.

Faisal, H.M.N., Katti, K.S., Katti, D.R., 2020. Modeling the behavior of organic kerogen in the proximity of calcite mineral by molecular dynamics simulations. Energy & Fuels 34(3), 2849-2860

542 Ferrage, E., Lanson, B., Sakharov, B. A., & Drits, V. A. 2005. Investigation of smectite
543 hydration properties by modeling experimental X-ray diffraction patterns: Part I.
544 Montmorillonite hydration properties. American Mineralogist 90(8-9), 1358-1374.

545 Fu, Y.T., Zartman, G.D., Yoonessi, M., Drummy, L.F., Heinz, H., 2011. Bending of Layered
546 Silicates on the Nanometer Scale: Mechanism, Stored Energy, and Curvature Limits.
547 Journal of Physical Chemistry C 115, 22292-22300.

548

549 Grim, R.E., 1942. Modern concepts of clay materials. Journal of Geology 50, 225-275.

550

551 Grim, R.E., 1968. Clay Mineralogy McGraw-Hill. New York, 206.

552 Guggenheim, S., Martin, R.T., 1996. Reply to the comment by DM Moore on "Definition of
553 clay and clay mineral: Joint report of the AIPEA nomenclature and CMS
554 nomenclature committees". Clays and Clay Minerals 44, 713-715.

555

556 Heinz, H., Koerner, H., Anderson, K.L., Vaia, R.A., Farmer, B.L., 2005. Force field for mica-
557 type silicates and dynamics of octadecylammonium chains grafted to montmorillonite.
558 Chemistry of Materials 17, 5658-5669.

559

560 Heinz, H., Suter, U.W., 2004. Atomic charges for classical simulations of polar systems.
561 Journal of Physical Chemistry B 108, 18341-18352.

562

563 Helmy, A.K., Ferreiro, E.A., de Bussetti, S.G., 2003. The surface energy of montmorillonite.
564 Journal of Colloid and Interface Science 268, 263-265.

565

566 Hendricks, S.B., Jefferson, M.E., 1938. Structures of kaolin and talc-pyrophyllite hydrates
567 and their bearing on water sorption of the clays. American Mineralogist 23, 863-875.

568

569 Jonas, E.C., Oliver, R.M., 1967. Size and shape of montmorillonite crystallites. Clays Clay
570 Miner 15, 27-33.

571

572 Jullien, M., Raynal, J., Kohler, E., Bildstein, O., 2005. Physicochemical reactivity in clay-rich
573 materials: Tools for safety assessment. Oil & Gas Science and Technology-Revue D
574 Ifp Energies Nouvelles 60, 107-120.

575

576 Karaborni, S., Smit, B., Heidug, W., Urai, J., vanOort, E., 1996. The swelling of clays:
577 Molecular simulations of the hydration of montmorillonite. Science 271, 1102-1104.

578

579 Katti, D., Shanmugasundaram, V., 2001. Influence of swelling on the microstructure of
580 expansive clays. Can. Geotech. J. 38, 175-182.

581

582 Katti, D.R., Ghosh, P., Schmidt, S., Katti, K.S., 2005a. Mechanical properties of the sodium
583 montmorillonite interlayer intercalated with amino acids. Biomacromolecules 6, 3276-
584 3282.

585

586 Katti, D.R., Katti, K.S., Thapa, K., Faisal, N., Modeling the Nanoscale Kerogen Inclusions in
587 Green River Oil Shale, Poromechanics VI, pp. 1968-1975.

588

589 Katti, D.R., Matar, M.I., Katti, K.S., Amarasinghe, P.M., 2009. Multiscale modeling of
590 swelling clays: A computational and experimental approach. Ksce Journal of Civil
591 Engineering 13, 243-255.

592

593 Katti, D.R., Patwary, Z.R., Katti, K.S., 2017a. Modelling clay-fluid interactions in
594 montmorillonite clays. Environmental Geotechnics 4, 322-338.

595

596 Katti, D.R., Schmidt, S.R., Ghosh, P., Katti, K.S., 2005b. Modeling the response of
597 pyrophyllite interlayer to applied stress using steered molecular dynamics. Clays and
598 Clay Minerals 53, 171-178.

599 Katti, D.R., Schmidt, S.R., Ghosh, P., Katti, K.S., 2007. Molecular modeling of the
600 mechanical behavior and interactions in dry and slightly hydrated sodium
601 montmorillonite interlayer. Can. Geotech. J. 44, 425-435.

602

603 Katti, D.R., Srinivasamurthy, L., Katti, K.S., 2015. Molecular modeling of initiation of
604 interlayer swelling in Na-montmorillonite expansive clay. Can. Geotech. J. 52, 1385-
605 1395.

606

607 Katti, D.R., Thapa, K.B., Katti, K.S., 2017b. Modeling molecular interactions of sodium
608 montmorillonite clay with 3D kerogen models. Fuel 199, 641-652.

609

610 Katti, D.R., Thapa, K.B., Katti, K.S., 2018. The role of fluid polarity in the swelling of
611 sodium-montmorillonite clay: A molecular dynamics and Fourier transform infrared
612 spectroscopy study. Journal of Rock Mechanics and Geotechnical Engineering 10,
613 1133-1144.

614

615 Katti, K.S., Sikdar, D., Katti, D.R., Ghosh, P., Verma, D., 2006. Molecular interactions in
616 intercalated organically modified clay and clay-polycaprolactam nanocomposites:
617 Experiments and modeling. Polymer 47, 403-414.

618

619 Katti, R.K., Katti, D.R., Katti, A.R., 2002. Behaviour of saturated expansive soil and control
620 methods. Balkema, Lisse [Netherlands]; Exton, PA.

621

622 Keller, L.M., Schuetz, P., Erni, R., Rossell, M.D., Lucas, F., Gasser, P., Holzer, L., 2013.
623 Characterization of multi-scale microstructural features in Opalinus Clay.
624 Microporous and Mesoporous Materials 170, 83-94.

625

626 Likos, W.J., Wayllace, A., 2010. POROSITY EVOLUTION OF FREE AND CONFINED
627 BENTONITES DURING INTERLAYER HYDRATION. Clays and Clay Minerals
628 58, 399-414.

629

630 Lin, J. J., Cheng, I. J., Wang, R. C., & Lee, R. J., 2001. Tailoring basal spacings of
631 montmorillonite by poly(oxyalkylene)diamine intercalation. Macromolecules 34(26),
632 8832-8834.

633

634 Liu, H., Chaudhary, D., Yusa, S.-i., & Tadé, M. O., 2011. Glycerol/starch/Na+-
635 montmorillonite nanocomposites: A XRD, FTIR, DSC and 1H NMR study.
636 Carbohydrate Polymers, 83(4), 1591-1597.

637

638 Lloret, A., Villar, M.V., Sanchez, M., Gens, A., Pintado, X., Alonso, E.E., 2003. Mechanical
639 behaviour of heavily compacted bentonite under high suction changes. Geotechnique
640 53, 27-40.

641

642 Massat, L., Cuisinier, O., Bihannic, I., Claret, F., Pelletier, M., Masrouri, F., Gaboreau, S.,
643 2016. Swelling pressure development and inter-aggregate porosity evolution upon
644 hydration of a compacted swelling clay. Applied Clay Science 124, 197-210.

645

646 Mishra, R.K., Mohamed, A.K., Geissbuhler, D., Manzano, H., Jamil, T., Shahsavari, R.,

647 Kalinichev, A.G., Galmarini, S., Tao, L., Heinz, H., Pellenq, R., van Duin, A.C.T., Parker,
648 S.C., Flatt, R.J., Bowen, P., 2017. cemff: A force field database for cementitious
649 materials including validations, applications and opportunities. Cement and Concrete
650 Research 102, 68-89.

651 Neaman, A., Pelletier, M., Villieras, F., 2003. The effects of exchanged cation, compression,
652 heating and hydration on textural properties of bulk bentonite and its corresponding
653 purified montmorillonite. Applied Clay Science 22, 153-168.

654

655 Norrish, K., 1954. The swelling of montmorillonite. Discussions of the Faraday society 18,
656 120-134.

657

658 Payne, M.C., Teter, M.P., Allan, D.C., Arias, T.A., Joannopoulos, J.D., 1992. Iterative
659 minimization techniques for abinitio total-energy calculations - molecular-dynamics
660 and conjugate gradients. Reviews of Modern Physics 64, 1045-1097.

661

662 Pellet, F.L., Keshavarz, M., Boulon, M., 2013. Influence of humidity conditions on shear
663 strength of clay rock discontinuities. Engineering Geology 157, 33-38.

664

665 Perdrial, J.N., Warr, L.N., 2011. Hydration behavior of mx80 bentonite in a confined-volume
666 system: implications for backfill design. Clays and Clay Minerals 59, 640-653.

667

668 Phillips, J.C., Braun, R., Wang, W., Gumbart, J., Tajkhorshid, E., Villa, E., Chipot, C., Skeel,
669 R.D., Kale, L., Schulten, K., 2005. Scalable molecular dynamics with NAMD. Journal
670 of Computational Chemistry 26, 1781-1802.

671

672 Pradhan, S.M., Katti, K.S., Katti, D.R., 2015. Evolution of Molecular Interactions in the
673 Interlayer of Na-Montmorillonite Swelling Clay with Increasing Hydration.
674 International Journal of Geomechanics 15.

675

676 Pusch, R., Karnland, O., Hökmark, H., 1990. GMM-a general microstructural model for
677 qualitative and quantitative studies of smectite clays. Swedish Nuclear Fuel and Waste
678 Management Co.

679

680 Pusch, R., Yong, R., 2003. Water saturation and retention of hydrophilic clay buffer -
681 microstructural aspects. Applied Clay Science 23, 61-68.

682

683 Rahromostaqim, M., Sahimi, M., 2018. Molecular Dynamics Simulation of Hydration and
684 Swelling of Mixed-Layer Clays. Journal of Physical Chemistry C 122, 14631-14639.

685

686 Rajini, N., Jappes, J.T.W., Jeyaraj, P., Rajakarunakaran, S., Bennet, C., 2013. Effect of
687 montmorillonite nanoclay on temperature dependence mechanical properties of
688 naturally woven coconut sheath/polyester composite. Journal of Reinforced Plastics
689 and Composites 32, 811-822.

690

691 Salles, F., Beurroies, I., Bildstein, O., Jullien, M., Raynal, J., Denoyel, R., Van Damme, H.,
692 2008. A calorimetric study of mesoscopic swelling and hydration sequence in solid
693 Na-montmorillonite. Applied Clay Science 39, 186-201.

694

695 Salles, F., Douillard, J.-M., Denoyel, R., Bildstein, O., Jullien, M., Beurroies, I., Van Damme,
696 H., 2009. Hydration sequence of swelling clays: Evolutions of specific surface area
697 and hydration energy. Journal of Colloid and Interface Science 333, 510-522.

698

699 Schmidt, S.R., Katti, D.R., Ghosh, P., Katti, K.S., 2005. Evolution of mechanical response of
700 sodium montmorillonite interlayer with increasing hydration by molecular dynamics.
701 Langmuir 21, 8069-8076.

702

703 Shroll, R.M., Smith, D.E., 1999. Molecular dynamics simulations in the grand canonical
704 ensemble: Application to clay mineral swelling. Journal of Chemical Physics 111,
705 9025-9033.

706

707 Sikdar, D., Pradhan, S.M., Katti, D.R., Katti, K.S., Mohanty, B., 2008. Altered phase model
708 for polymer clay nanocomposites. Langmuir 24, 5599-5607.

709

710 Skipper, N.T., Chang, F.R.C., Sposito, G., 1995a. Monte-carlo simulation of interlayer
711 molecular-structure in swelling clay-minerals .1. Methodology. Clays and Clay
712 Minerals 43, 285-293.

713

714 Skipper, N.T., Sposito, G., Chang, F.R.C., 1995b. Monte-carlo simulation of interlayer
715 molecular-structure in swelling clay-minerals .2. Monolayer hydrates. Clays and Clay
716 Minerals 43, 294-303.

717

718 Smith, D.E., Wang, Y., Whitley, H.D., 2004. Molecular simulations of hydration and swelling
719 in clay minerals. Fluid Phase Equilibria 222, 189-194.

720

721 Sposito, G., Prost, R., 1982. STRUCTURE OF WATER ADSORBED ON SMECTITES.
722 Chemical Reviews 82, 553-573.

723

724 Sun, L., Tanskanen, J.T., Hirvi, J.T., Kasa, S., Schatz, T., Pakkanen, T.A., 2015. Molecular
725 dynamics study of montmorillonite crystalline swelling: Roles of interlayer cation
726 species and water content. Chemical Physics 455, 23-31.

727

728 Tao, L., Tian, X.-F., Yu, Z., Tao, G., 2010. Swelling of K+, Na+ and Ca2+-montmorillonites
729 and hydration of interlayer cations: a molecular dynamics simulation. Chinese Physics
730 B 19.

731

732 Teppen, B.J., Rasmussen, K., Bertsch, P.M., Miller, D.M., Schafer, L., 1997. Molecular
733 dynamics modeling of clay minerals .1. Gibbsite, kaolinite, pyrophyllite, and
734 beidellite. Journal of Physical Chemistry B 101, 1579-1587.

735

736 Thapa, K.B., Katti, K.S., Katti, D.R., 2020. Compression of Na-Montmorillonite Swelling
737 Clay Interlayer Is Influenced by Fluid Polarity: A Steered Molecular Dynamics Study.
738 Langmuir : the ACS journal of surfaces and colloids.

739

740 Van Olphen, H., Fripiat, J.-J., 1979. Data handbook for clay materials and other non-metal lic
741 minerals: providing those involved in clay research and indus trial application with

sets of authoritative data describing the physical and chemical properties and mineralogical composition of the available reference materials.

Vanommeslaeghe, K., Hatcher, E., Acharya, C., Kundu, S., Zhong, S., Shim, J., Darian, E., Guvench, O., Lopes, P., Vorobyov, I., MacKerell, A.D., 2010. CHARMM General Force Field: A Force Field for Drug-Like Molecules Compatible with the CHARMM All-Atom Additive Biological Force Fields. Journal of Computational Chemistry 31, 671-690.

Villar, M.V., Lloret, A., 2004. Influence of temperature on the hydro-mechanical behaviour of a compacted bentonite. Applied Clay Science 26, 337-350.

Wang, C.y., Mao, N.h., Wu, F.T., 1979. The mechanical property of montmorillonite clay at high pressure and implications on fault behavior. Geophysical Research Letters 6, 476-478.

Yong, R.N., 1999. Soil suction and soil-water potentials in swelling clays in engineered clay barriers. Engineering Geology 54, 3-13.

Zartman, G.D., Liu, H., Akdim, B., Pachter, R., Heinz, H., 2010. Nanoscale Tensile, Shear, and Failure Properties of Layered Silicates as a Function of Cation Density and Stress. Journal of Physical Chemistry C 114, 1763-1772.

Figures

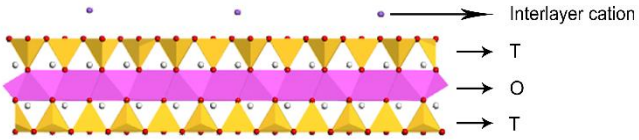

Fig. 1. Molecular model of 6×3 Na-montmorillonite clay mineral layer with interlayer cations **that is replicated to build the tactoid model**

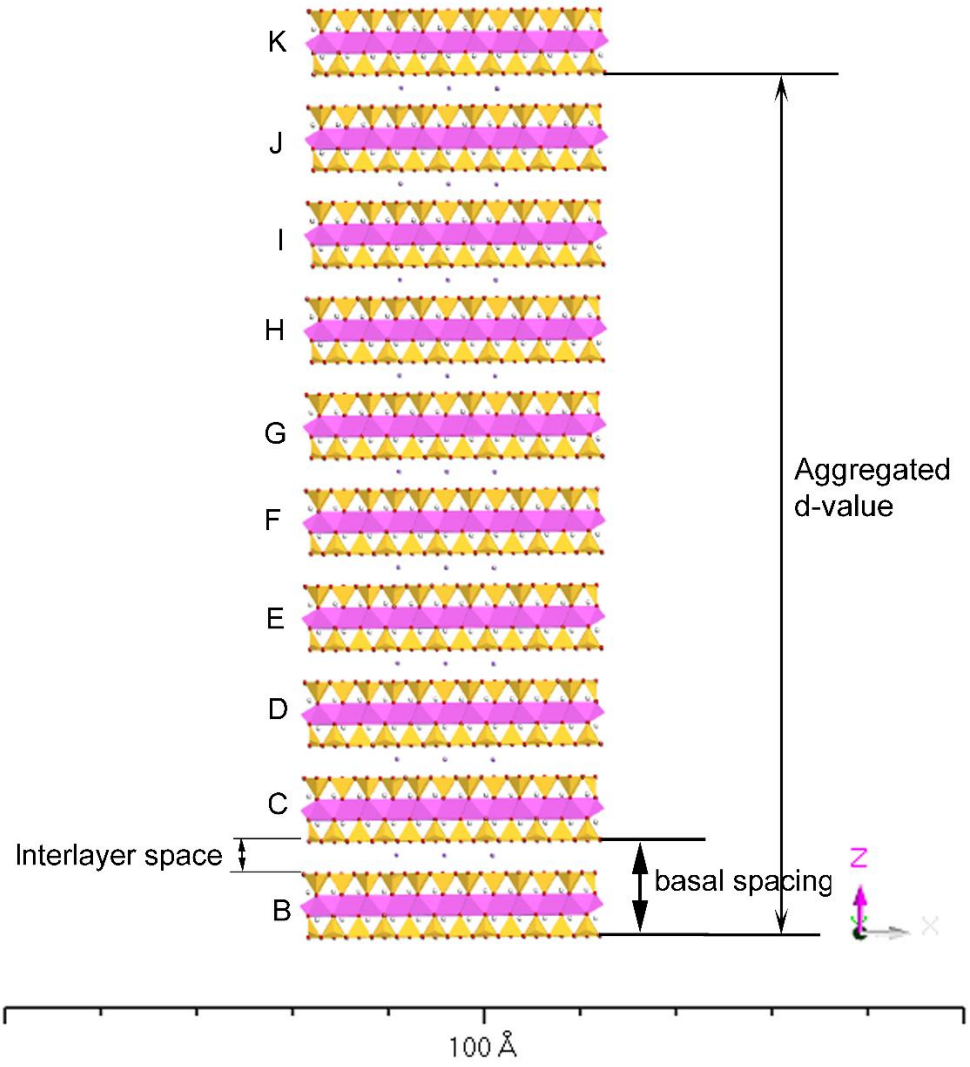

Fig. 2. Molecular model of Na-montmorillonite tactoid containing ten clay mineral layers. The bottom clay mineral layer was termed as the 'B" layer, and the top clay mineral layer was termed as the 'K' layer.

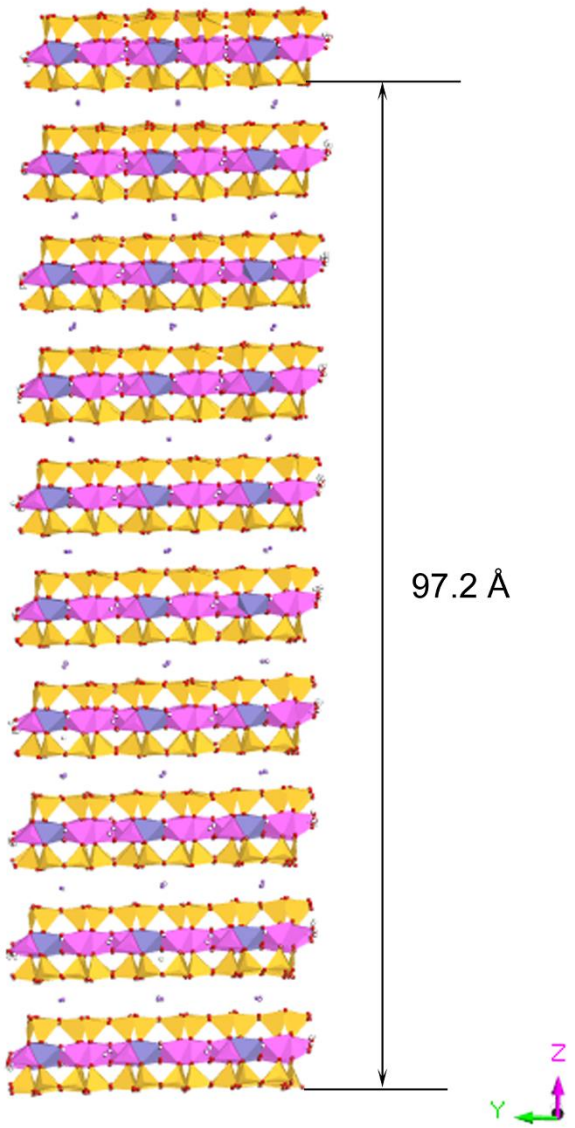

785
786
787 **Fig. 3.** NTP equilibrated model of Na-Mt tactoid.
788
789

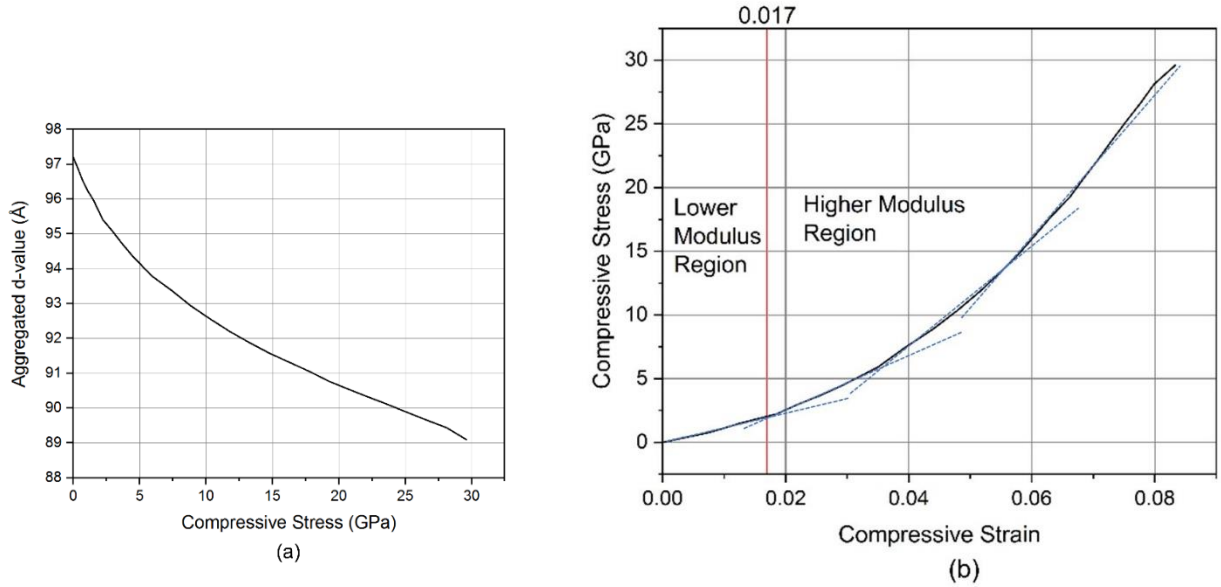

Fig.4. Plots showing (a) Aggregated d-value vs. compressive stress and (b) Compressive stress vs. strain of equilibrated Na-Mt tactoid. The vertical line at a strain value of 0.017 specifies the boundary of two different compressive strain behaviors (linear and nonlinear) inside tactoid.

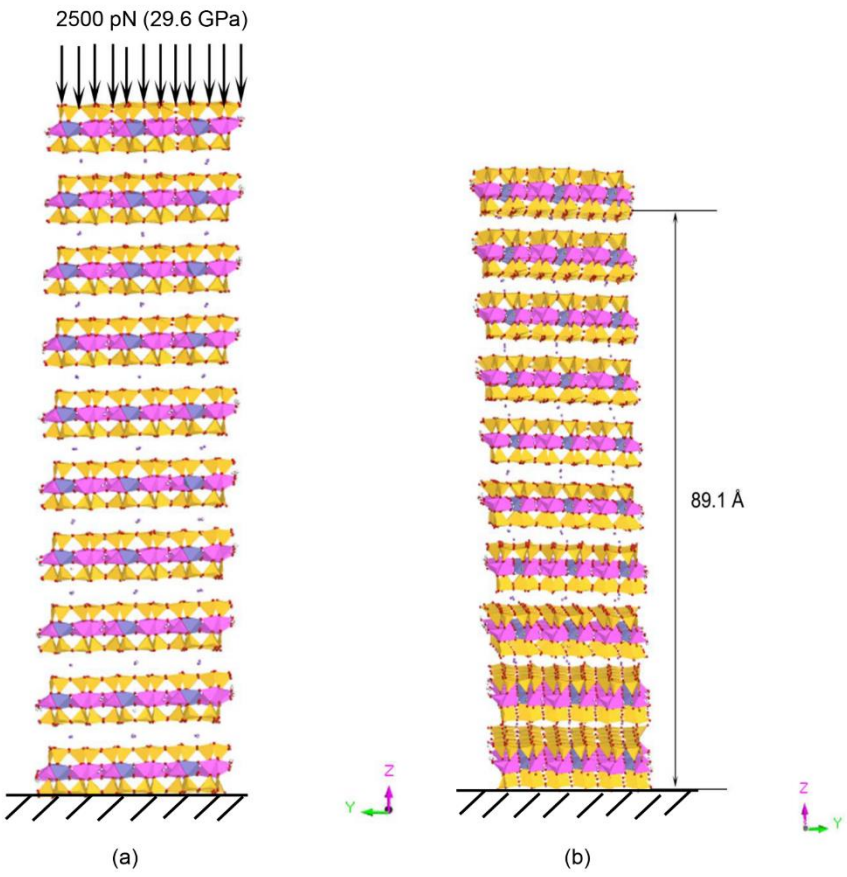

Fig. 5. Na-Mt tactoid under the compression of 29.6 GPa (a) initial condition, and (b) final condition.

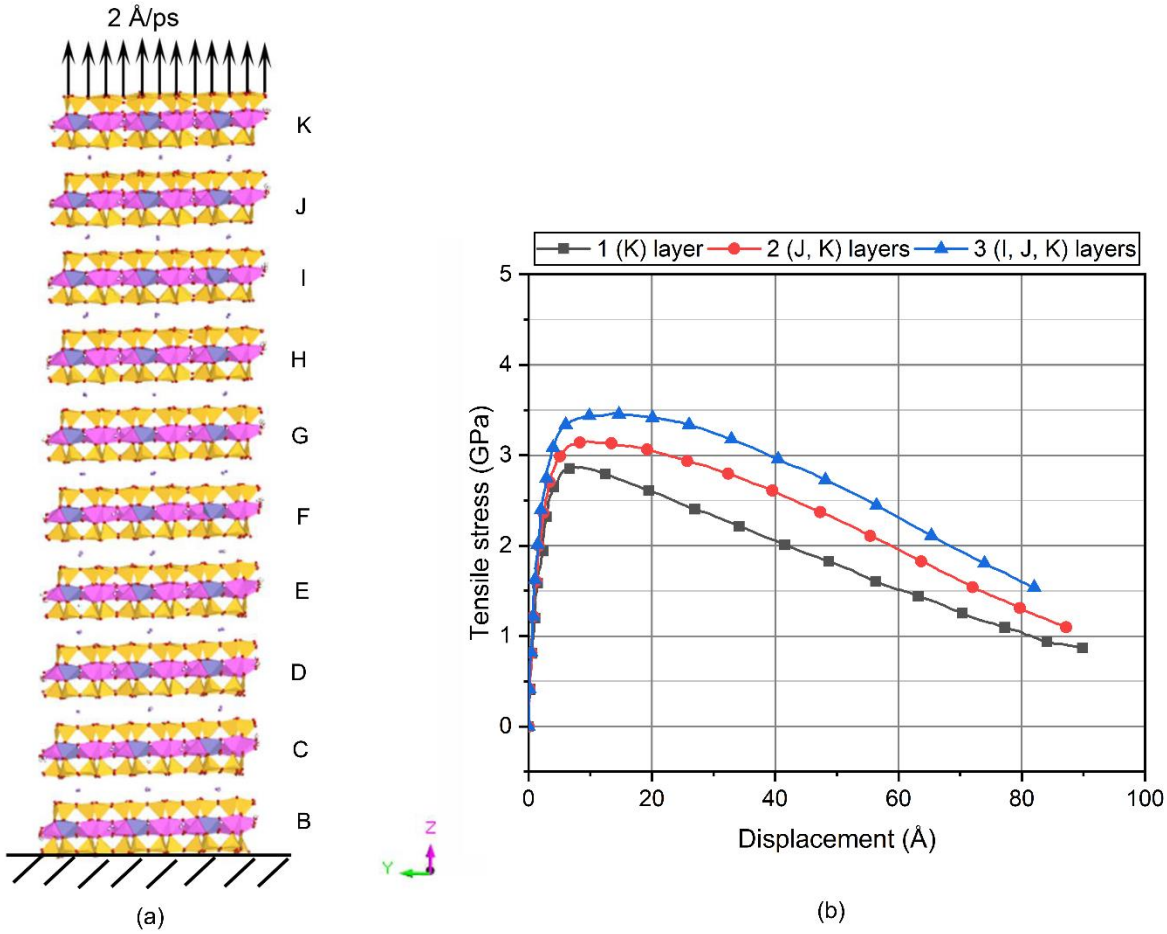

Fig. 6. (a) Vertical tensile pulling of top clay mineral layer, and (b) tensile stress vs. displacement plot for pulling top 1 (K), 2 (J, K), and 3 (I, J, and K) clay mineral layers.

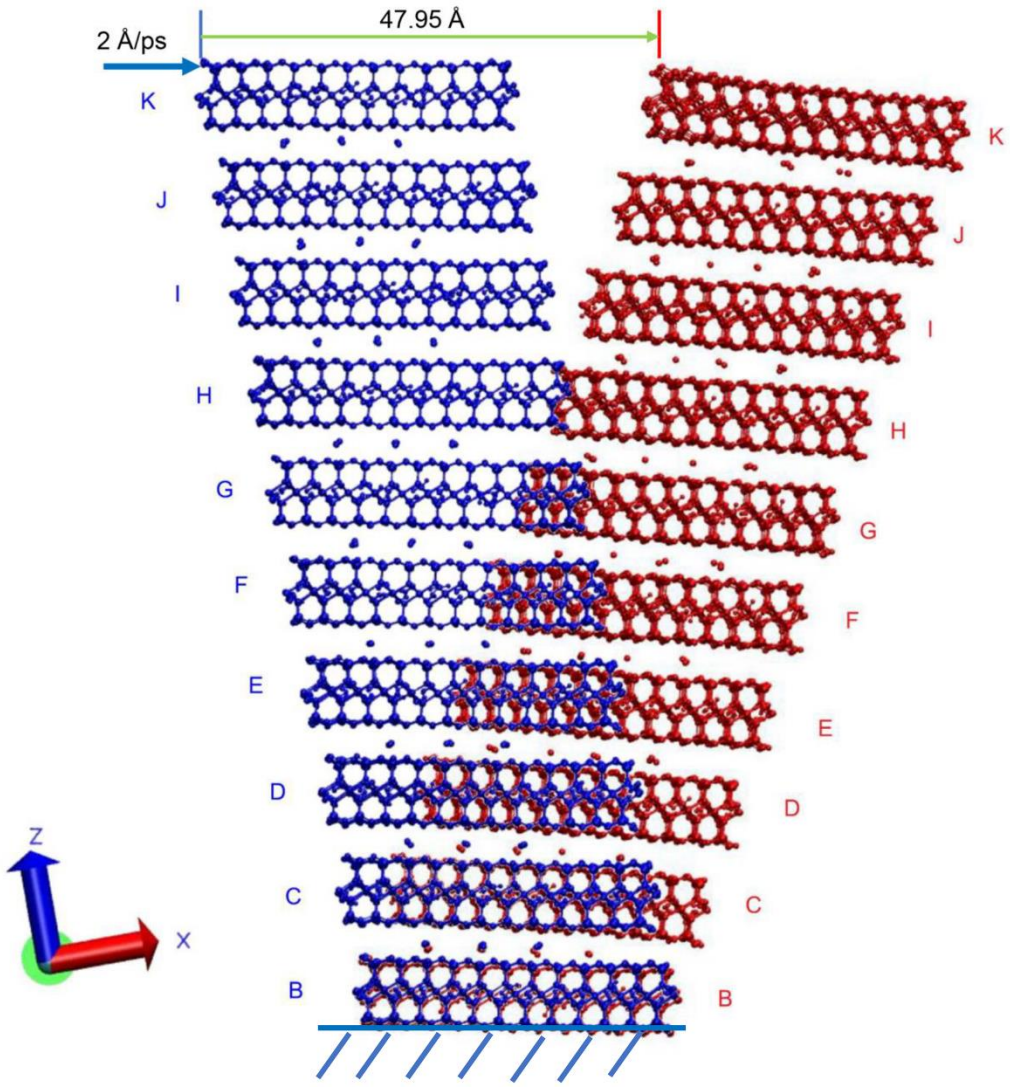

Fig. 7. Shearing of individual Na-Mt tactoid. The initial (left) and final (right) model of tactoid due to shearing is superimposed to indicate the extent of shearing.

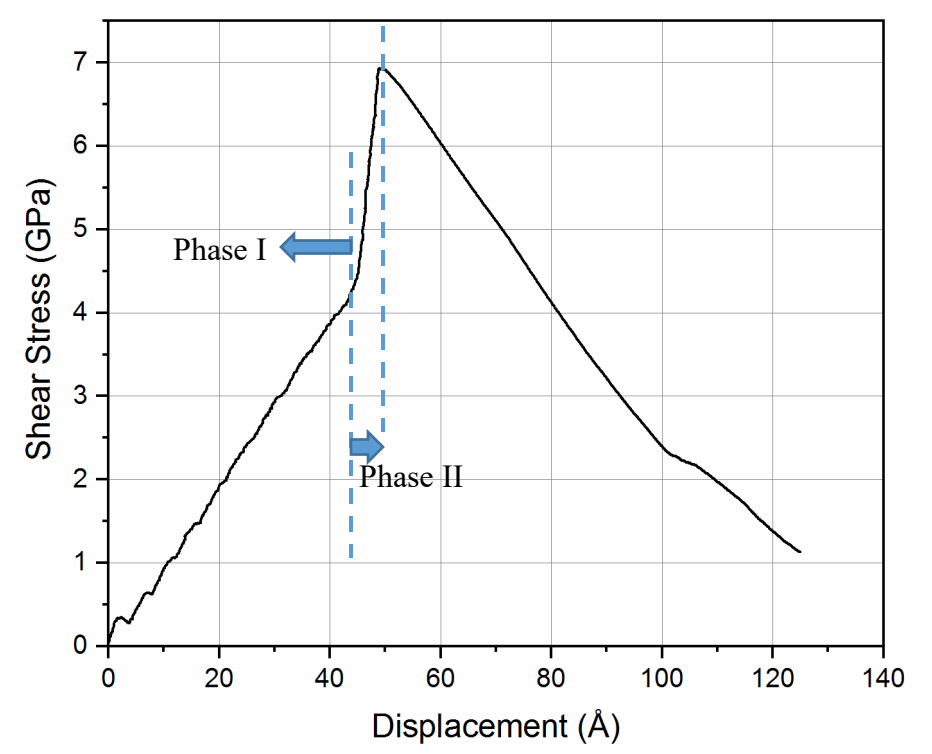

Fig. 8. Shear stress vs. displacement plot for the top clay (K) layer upon horizontal shearing of tactoid.

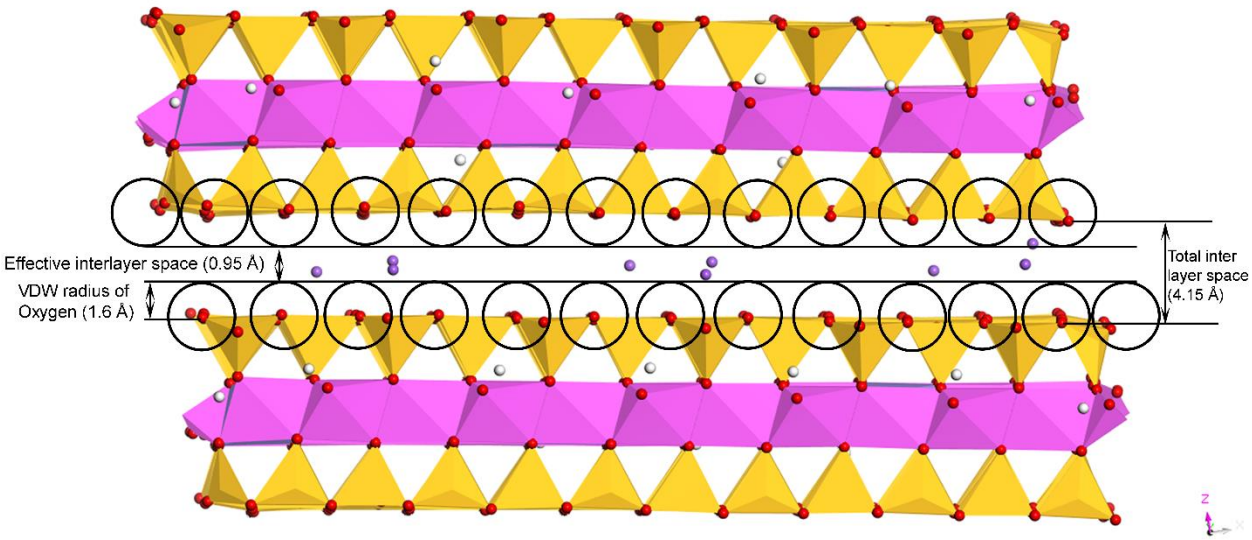

Fig. 9. Effective interlayer space of Na-Mt clay structure.

Tables

Table 1: Calculated d-values between clay mineral layers inside Na-Mt tactoid

Clay mineral layers pair	Equilibrated d-value (Å)
B-C	10.79
C-D	10.79
D-E	10.80
E-F	10.80
F-G	10.80
G-H	10.79
H-I	10.80
I-J	10.80
J-K	10.79

Table 2: Non-bonded energies (kJ/mol) between clay mineral layers in Na-Mt tactoid

Clay mineral layers pair	Electrostatic (kJ/mol)	VDW (kJ/mol)	Non-bonded (kJ/mol)
B-C	751	-2597	-1846
C-D	750	-2596	-1846
D-E	752	-2597	-1845
E-F	746	-2599	-1853
F-G	745	-2599	-1854
G-H	745	-2600	-1855
H-I	744	-2601	-1857
I-J	743	-2602	-1859
J-K	761	-2603	-1842

Table 3: Na-clay mineral layer interaction energy in Na-Mt tactoid

Clay-mineral layer	Electrostatic (kJ/mol)	VDW (kJ/mol)	Non-bonded (kJ/mol)
B	-3881	89	-3792
C	-6397	43	-6354
D	-6679	55	-6624
E	-6694	56	-6638
F	-6693	55	-6638
G	-6694	54	-6640
H	-6689	54	-6635
I	-6665	50	-6615
J	-6341	34	-6307
K	-3585	92	-3493

Table 4: Binding energy of each clay mineral layer to tactoid

Clay-mineral layer	Electrostatic (kJ/mol)	VDW (kJ/mol)	Non-bonded (kJ/mol)
B	-3140	-2511	- 5651
C	-5200	-5145	-10345
D	-5200	-5145	-10345
E	-5219	-5147	-10366
F	-5227	-5150	-10377
G	-5230	-5152	-10382
H	-5227	-5154	-10381
I	-5208	-5159	-10367
J	-4851	-5174	-10025
K	-2842	-2515	-5357

Table 5. Elastic moduli of a tactoid from compression simulations at various magnitudes of stress.

Stress Region (GPa)	Modulus (GPa)
0-2.22	125
2.22-5.92	237.5
5.92-14.8	411
14.8-29.6	643

852

853 **Table 6:** Calculated d-values between clay mineral layers inside Na-Mt tactoid under 29.6 GPa
854 compressive stress

Clay mineral layer pair	Equilibrated d-value (Å) under 29.6 GPa	Interlayer deformation (Å)
B-C	10.02	0.77
C-D	9.95	0.84
D-E	9.94	0.86
E-F	9.91	0.89
F-G	9.89	0.91
G-H	9.87	0.92
H-I	9.87	0.93
I-J	9.86	0.94
J-K	9.84	0.95

855
856
857
858
859
860
861
862
863
864
865 **Graphical Abstract**
866

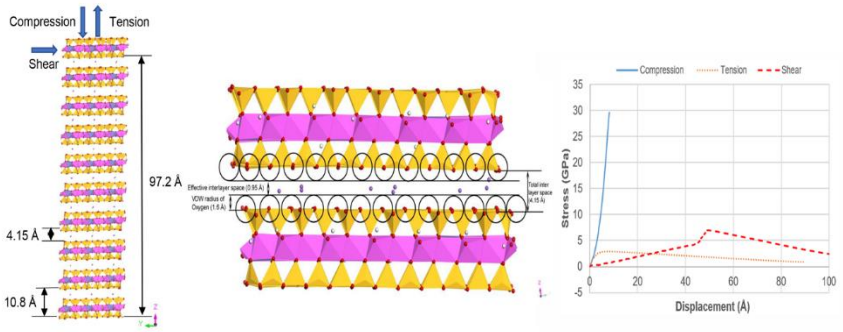

867